Chapter 14

Numerical Simulation of Passively Q-Switched Solid State Lasers

I. Lăncrănjan, R. Savastru, D. Savastru and S. Micloş

Additional information is available at the end of the chapter

http://dx.doi.org/10.5772/47812

1. Introduction

Short laser light pulses have a large number of applications in many civilian and military applications [1-10]. To a large percentage these short laser pulses are generated by solid state lasers using various active media types (crystals, glasses or ceramic) operated in Q-switching and/or mode-locking techniques [1-10]. Among the short light pulses laser generators, those operated in Q-switching regime and emitting pulses of nanosecond FWHM duration occupy a large part of civilian (material processing - for example: nano-materials formation by using ablation technique [3,7]) and military (projectile guidance over long distances and range finding) applications. Basically, Q-switching operation relies on a fast switching of laser resonator quality factor Q from a low value (corresponding to large optical losses) to a high one (representing low radiation losses). Depending on the proposed application, two main Q-switching techniques are used: active, based on electrical (in some cases operation with high voltages up to about 1 kV being necessary) or mechanical (spinning speeds up to about 1 kHz being used) actions on an optical component at least, coming from the outside of the laser resonator, and passive relying entirely on internal to the laser resonator induced variation of one optical component transmittance.

2. Theory

Figure 1 displays a general schematic of electronic energy levels of laser active centers embedded in an active medium and of saturable absorption centers embedded into solid state passive optical Q-switch cell laser oscillator operated in passive optical Q-switching regime [11-18,26]. As laser active centers, rare earth (RE) triple ions included by substitution into crystalline or poly micro-crystalline structure of the solid state active medium are used to a large extent. The four electronic energy levels of a laser active center can be observed together with the transitions between them, transitions which constitute the laser emission

cycle of the active medium. The pumping transition, sometimes denoted as pumping absorption, from level "am0" to level "am1" together with the laser emission transition from level "am2" to level "am3" are presented. The pumping transition which assures attaining the population inversion between levels "am2" and "am3" can be technologically realized, considering basically the longitudinal or transverse/perpendicular versus laser beam propagation direction, by absorption of pumping radiation using one of two possibilities: longitudinal, along the active medium axis or transverse, through its side surfaces. Usually longitudinal pumping means a distribution of population inversion density which has an important consequence upon the laser dynamics. The transitions "am1" → "am2" and "am3" → "am0" are fast non-radiative transitions [26]. The laser emission transition "am2" → "am3" has a characteristic fluorescence lifetime τ_g in the range from μs to ms. The three-levels structure of electronic energy laser active medium is possible with the main characteristic difference that the level "am3" is identical with the level "am0" [5,6,7].

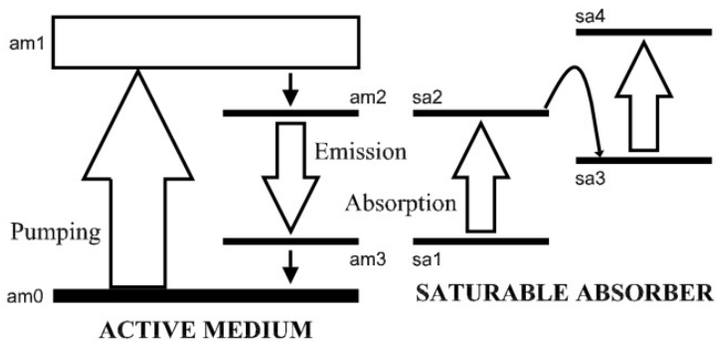

Figure 1. The schematic of a solid state laser active medium and passive optical Q-switch cell electronic energy levels. Active medium - levels: am0 - ground level; am1 - pumping level; am2 - upper laser level; am3 - lower laser level; Saturable absorber - sa1 - ground level; sa2 - upper saturable absorber level; sa3 - saturable absorber lower excited level; sa4 - saturable absorber upper excited level [26].

As can be seen in the schematic describing the functional cycle of the saturable absorber material, the absorption transition from electronic energy level "sa1" to electronic energy level "sa2" is the most important for passive optical Q-switching process, relying on its nonlinear characteristic absorption coefficient, $\alpha(I)$. The $\alpha(I)$ coefficient varies with the intensity I of the light beam incident on the saturable absorber according to an equation as [5,7]:

$$\alpha(I) = \frac{\alpha_0}{1 + \frac{I}{I_{sat}}} \tag{1}$$

I_{sat} represents the saturation value of the light beam intensity, the value for which the absorption coefficient is reduced with 50%. The function as a passive optical Q-switch cell is obtained by absorptive transition "sa1" → "sa2" which is characterized by a fluorescence lifetime of the upper level long enough to store the saturable absorption centres on the upper level and to depopulate the lower level at a fast rate. In this situation, the passive

optical Q-switch cell appears as transparent (bleached) at the laser wavelength, allowing the laser radiation to circulate inside resonator. It has to be understood that simultaneously with the bleaching process, in the active medium the population inversion is accumulated, the laser active centres being stored into upper laser level. Practically, the assemble of the pumped active medium and passive optical Q-switch cell placed inside a resonator formed by two mirrors represent a laser oscillator with poor optical quality and high threshold condition. When the high energy threshold condition is attained for this low quality oscillator, a large population inversion is stored in the active medium and enhanced fluorescence emission intensity at laser wavelength is obtained. Because of the passive optical Q-switch cell bleaching effect, which is fast enough with in comparison to the upper laser level fluorescence lifetime, the optical quality of the resonator is fast growing to high values allowing laser emission [11,12,19-23]. As a consequence, the population inversion accumulated in the active medium is converted into emission of short laser pulses. The laser oscillator behaves as in free running regime in a very short early period quality and after that as in Q-switching regime characterised by emission of a short laser pulse burst.

As can be noticed, the possible situation of a non-saturable parasitic absorption of the passive optical Q-switch cell is presented. This parasitic absorption can take place between levels "sa3" and "sa4", levels "sa3" being populated by excitation transfer process from level "sa2" [20,21,27]. The non-saturable parasitic absorption can represent an embarrassment for Q-switching process in the case of a good spectral match between laser emission wavelength and "sa3" $\rightarrow$ "sa4" absorption because imposing a lower quality of the laser resonator after the bleaching of the passive optical Q-switch cell [13-16].

2.1. Laser rate equations

The parameters characteristic for a passively optical Q-switched operated solid state laser system and appearing in the equations describing its functionality, as schematically presented in Figure 2 and in Figure 5, are the following:

- Φ -the laser photon density;
- Φ_P -the laser pumping photon density;
- N_g - the population inversion density;
- N_a -the instantaneous population density of the SA ground absorbing state;
- N_{a0} -the total population density of the SA;
- l_g -the length of the gain medium;
- l_a -the length of the SA;
- c - the speed of light;
- R_p -the pumping rate of the active medium;
- K_a -the pumping radiation absorption coefficient of the active medium;
- R_1 -the reflectivity of the rear (high reflectance) laser mirror;
- R_2 -the reflectivity of the output coupler;
- L -the round trip non-saturable dissipative optical loss;
- σ_g -the stimulated emission cross section area of the gain medium;

- σ_a -the ground electronic state absorption cross section of the SA;
- σ_{ae} -the excited electronic state absorption cross section of the SA;
- τ_r -the light round trip transit time in the laser resonator;
- τ_g - the lifetime of the upper laser level of the gain medium;
- τ_a - the lifetime of the SA excited state;
- S_a -the beam cross-section area in the passive optical Q-switch cell;
- S_g -the beam cross-section area in the active medium;
- S -the pumped active medium contribution to priming spontaneous emission at the laser wavelength.

Without losing the generality degree of the mathematical approach, the photons of the laser beam are supposed to follow a Gaussian distribution in planes transverse to the laser beam optic axis, being defined as [24-26,31]:

$$\Phi(r,t) = \Phi(0,t)\exp\left(-\frac{2r^2}{w_L^2}\right) \tag{2}$$

Also without losing the generality degree of the mathematical approach, the photons of the pumping beam are supposed to follow a Gaussian distribution in planes transverse to the laser beam optic axis, being defined as [24-26,31]:

$$\Phi_P(r,t) = \Phi_P(0,t)\exp\left(-\frac{2r^2}{w_P^2}\right) \tag{3}$$

In the laser rate equation approach, Φ, N_g and N_a as functions of time are obtained by numerically solving a system of coupled differential equation. Whatever which is the used integration method, the accuracy of the solution is improved by considering physics details as intimate as possible, which means to take into account the overall purpose of the numerical performed investigation and the limits imposed by the electronic machine. In other words, an improved efficiency of the numerical simulation is a desirable purpose. Among the intimate physics details to be considered, the spatial distributions of Φ, N_g and N_a are important. By considering a cylindrical coordinate system r, Φ and z, properly suited to usual laser resonator geometry and its cylindrical symmetry, Φ, N_g and N_a are defined as functions of r and t. The Φ, N_g and N_a variations with z, the laser resonator axis coordinate are not directly considered, the implicitly ones being possible. Equations (4), (5) and (6) form a system of differential rate equations defining Φ, N_g and N_a. The system of equations (4), (5) and (6) can be numerically solved using different methods, mostly Runge-Kutta-Fehlberg [11-22,26]. It is important to underline a fact which will be demonstrated by experimentally results in the followings: the output parameters of a passively Q-switched solid state laser have large variations over very short periods before and/or after long time duration characterized by slow or zero such variations. Connected to this observation, it is worth to underline the necessity of accurate definition of the role of each term which appears in these equations. Equation (4) defines the time variation of laser photon density inside laser

resonator as a sum of contributions due to amplification (gain) along the active medium, saturable losses ("sa1" → "sa2" transition in Figure 1) and parasitic losses ("sa3" → "sa4" transition in Figure 1) of the passive optical Q-switch cell, parasitic and output (R_1, R_2) laser resonator losses (L) and fluorescence emission at laser wavelength. In Equation (4), the integration over radial coordinate r is to be noticed.

$$\int_0^{\infty} \frac{\partial \Phi(r,t)}{\partial t} \cdot 2\pi r \cdot dr = \int_0^{\infty} \frac{\Phi(r,t)}{\tau_r} \left[2\sigma_g l_g N_g(r,t) - 2\sigma_a l_a N_a(r,t) - L_{par}(r,t) + \ln(R_1 R_2) - L + S(r,t) \right] \cdot 2\pi r \cdot dr \,. \tag{4}$$

Equation (5) defines the variation speed of the population inversion density as a sum of contributions due to the processes occurring in the active medium, namely stimulated emission, depopulation of upper laser level "am2" caused by fluorescence emission of an intensity proportional to $1/\tau_g$ and a positive term representing the pumping rate [31]:

$$\frac{dN_g(r,t)}{dt} = -c\sigma_g l_g \Phi(r,t) N_g(r,t) - \frac{N_g(r,t)}{\tau_g} + R_p(r,t) \tag{5}$$

Equation (6) defines the variation speed of the saturable absorber centres situated in the ground level "sa1" population inversion density as a sum of contributions due to the processes occurring in the passive optical Q-switch cell, namely absorption at laser wavelength (transition "sa1" → "sa2"), depopulation of first excited level "sa2" caused by fluorescence emission and/or non-radiative transitions of an intensity proportional to $1/\tau_a$:

$$\frac{dN_a(r,t)}{dt} = -\frac{S_g}{S_a} \gamma c \sigma_a l_a \Phi(r,t) N_a(r,t) + \frac{N_{ao} - N_a(r,t)}{\tau_a} \tag{6}$$

In Equation (4), the role of non-saturable losses of the passive optical Q-switch cell due to "sa3" → "sa4" absorption is considered by introducing the term L_{par} which is defined using σ_{ae} as [18,30,31]:

$$L_{par}(r,t) = 2\sigma_{ae} \left[N_{ao} - N_a(r,t) \right] \tag{7}$$

In Equation (5), the rate term $R_p(r,t)$ represents absorption of pumping radiation into active medium and is defined as:

$$R_P(r,t) = K_{abs} \int_0^{\infty} \Phi_P(0,t) 2\pi r dr \tag{8}$$

The coupled differential equations system (4), (5) and (6) is an Initial Value Problem (IVP). Accurate definitions of photon density, population inversion and saturable absorption centres population density initial values represent a key point of passive optical Q-switched solid state

laser numerical simulation. The initial value of the laser photon density can be considered as proportional to the active medium fluorescence emission intensity. When the differential equation system (4), (5) and (6) is solved numerically, for practical reasons, photon density initial value is defined as a much smaller percentage of its maximum value [6,26,31]:

$$S(r,0) \approx k\Phi_m(r,t) \tag{9}$$

The initial value of the population inversion density in the active medium is defined as

$$N_g(r,0) = N_g(0,0)\exp\left(-\frac{2r^2}{w_P^2}\right) \tag{10}$$

In Equation (10) the factor $N_g(0,0)$, a factor which represents the laser oscillation threshold condition on the laser resonator axis ($r = 0$), being possible denoted as an "axial" threshold condition is defined as:

$$N_g(0,0) = \frac{\ln\left(\frac{1}{R_1R_2}\right) + \left(\frac{\sigma_{ae}}{\sigma_a}\right)\ln\left(\frac{1}{T_0^2}\right) + L}{2\sigma_g l_g}\left(1 + \frac{w_L^2}{w_P^2}\right) \tag{11}$$

The initial value of saturable absorption centres population density is most easily to define because, as a simplification corresponding to most encountered experimental configurations, these centres are uniformly distributed inside the passive optical Q-switch cell. The initial value of saturable absorption centres population density is defined as:

$$N_a(r,0) = N_{ao} \tag{12}$$

A possible development of mathematical apparatus used for numerical simulation passive optical Q-switched solid state laser can be obtained by substituting equations (2), (10) and (12) into (5) and (6) which are modified into:

$$N_g(r,t) = N_g(0,0)\exp\left(-\frac{2r^2}{w_P^2}\right)\exp\left[-\gamma c\sigma_g \exp\left(-\frac{2r^2}{w_L^2}\right) l_g \int_0^t \Phi(0,t)dt\right], \tag{13}$$

$$N_a(r,t) = N_{ao}\exp\left[-\frac{S_g}{S_a}\sigma_a c \exp\left(-\frac{2r^2}{w_L^2}\right)\int_0^t \Phi(0,t)dt\right] \tag{14}$$

In the next step, by substituting equations (2), (13) and (14) into (4), an equation describing photon density speed of variation can be obtained:

$$\frac{d\Phi(0,t)}{dt} = \frac{4\sigma_g N_g(0,0) l_g \Phi(0,t)}{w_L^2 \tau_r} K_1(t) - \frac{4(\sigma_a - \sigma_{ae}) N_{a0} l_a \Phi(0,t)}{w_L^2 \tau_r} K_2(t) - \frac{\Phi(0,t)}{\tau_r} K_3 \tag{15}$$

In Equation (15) the factors $K_1(t)$, $K_2(t)$ and K_3 are introduced for ease of numerical integration, of numerical solving procedures. These factors are defined as:

$$K_1(t)=\int_0^{\infty}\exp\left[-\gamma\sigma_g c\exp\left(-\frac{2r^2}{w_L^2}\right)\int_0^t\Phi(0,t)dt\right]\exp\left[-2\frac{r^2\left(w_L^2+w_P^2\right)}{w_L^2w_P^2}\right]2rdr\,, \tag{16}$$

$$K_1(t)=\int_0^{\infty}\exp\left[-\frac{S_g}{S_a}\sigma_a c\exp\left(-\frac{2r^2}{w_L^2}\right)\int_0^t\Phi(0,t)dt\right]\exp\left[-\frac{2r^2}{w_L^2}\right]2rdr\,, \tag{17}$$

$$K_3=\ln\left(\frac{1}{R_1R_2}\right)+\left(\frac{\sigma_{ae}}{\sigma_a}\right)\ln\left(\frac{1}{T_0^2}\right)+L \tag{18}$$

In defining K_3, the initial small-signal transmission of the passive optical Q-switch cell is used being defined as:

$$T_0=\exp\left(-\sigma_a l_a N_{a0}\right) \tag{19}$$

For practical reasons, for comparison of experimental results with the ones obtained by numerically solving the rate coupled differential equations, a simplification was considered, namely that of a transverse to the active medium uniform pumping. Regarding the above developed mathematical apparatus, this hypothesis is equivalent to considering that pumping radiation has a distribution with $w_P \to \infty$. A direct consequence of this simplification is that while the photon density and saturable absorption centres population density initial values are kept the same, population inversion density initial value is modified as:

$$N_g(0,0)=\frac{\ln\left(\frac{1}{R_1R_2}\right)+\ln\left(\frac{1}{T_0^2}\right)+L}{2\sigma_g l_g} \tag{20}$$

The coupled differential equations system (4), (5) and (6) is simplified to:

$$\frac{d\Phi(t)}{dt}=\frac{\Phi(t)}{\tau_r}\left[2\sigma_g l_g N_g(t)-2\sigma_a l_a N_a(t)+\ln(R_1\cdot R_2)-L\right]+S\,, \tag{21}$$

$$\frac{dN_g}{dt}=-c\sigma_g l_g\varphi N_g-\frac{N_g}{\tau_g}+R_p\,, \tag{22}$$

$$\frac{dN_a}{dt}=-c\sigma_a l_a\varphi N_a+\frac{N_{ao}-N_a}{\tau_a}\,. \tag{23}$$

2.2. Iteration technique

The main idea of passive optical Q-switched solid state laser using an iteration technique consists in considering a Gaussian distribution of photon density inside laser resonator; launching it inside laser resonator at an initial, reference plane transverse to the laser beam axis; calculating its modification during round trip propagation between the laser mirrors using the ABCD matrix M_{LR} characteristic for the investigated laser resonator [36-38]. The integral equation representing the imposed condition of photon density distribution reproducibility in phase and amplitude, with the exception of a proportionality coefficient, is defined at the chosen reference plane by numeric integration corresponding to round trip propagation [9,28-30]. The numeric integration corresponding to round trip propagation is iteratively calculated for verifying that photon density distribution reproducibility is attained.

Such approach can conduct to determination of the fundamental mode parameters of the laser cavity under real pumping conditions, assuming a Gaussian distribution of pumping radiation intensity [37]. The radially variable gain profiles [32-34] as well as heat-source densities [35] which occur as a result of focusing of the pump beam in the majority of diode-pumped lasers can be considered. In analyzing this type of laser in the framework of the space-dependent rate-equation model [32-37], we assume that laser mode parameters are known a priori. The thermal guiding effect responsible for mode structure in lasers operating near threshold can be analyzed establishing its importance. Thus the developed complementary models that account for gain guiding [32,35], the Kerr effect [34], and gain-related effects [32-37] can be developed.

Mathematically, the above mentioned considerations can be expressed by differential equation defining the propagation of photon density distribution along the laser resonator axis, z being the axial coordinate:

$$\frac{1}{I_r(z)}\frac{dI_r(z)}{dz}=\frac{g(z)}{1+I_r(z)} \tag{24}$$

In Equation (24), $g(z)$ is the small-signal logarithmic gain coefficient and $I_r(z)$ is relative laser beam density defined as:

$$I_r(z)=\frac{I(z)}{I_{sat}} \tag{25}$$

I_{sat} represents the saturation intensity of the investigated laser active medium and resonator.

As mentioned previously, at the starting point the cavity matrix M_{LR} including the effective thermal lensing power of a gain medium is calculated in order to determine the incident Gaussian beam profile at the considered point of entrance (reference plane). It is considered a small value of the incident intensity magnitude compared with the saturation one. In each step of the iterative procedure the output intensity profile after passage through the gain medium is calculated according to Equations (24) and (25) as:

$$I_{r,1}\exp\left(I_{r,1}\right)=I_{r,0}\exp\left(gl_rI_{r,0}\right) \tag{26}$$

where $I_{r,1}$ is the output laser beam intensity at the reference plane and $I_{r,0}$ is the input counterpart incident on the reference plane. Equation (26) can be transformed into a Lambert W function [38]:

$$I_{r,1}=W\left[I_{r,0}\exp\left(I_{r,0}\right)G\left(l_r\right)\right] \tag{27}$$

Equation (27) can be solved using by Lambert W function tables. The general integral of this type of first-order ordinary differential equation is known as the Lambert W function.

The cavity matrix M_{LR} is defined as the product of active medium effective gain matrix M_{SG}, bare cavity M_{BC} which includes the rest of laser resonator components. The laser beam is passed through the cavity, applying the product of both matrices M_{SG} and M_{BC}. At each step we introduce the logarithmic passive losses of cavity δ_{pas}, multiplying the intensity profile at the output mirror by the factor $\exp(-\delta_{pas})$. Because of the saturated gain profile and passive losses, the peak intensity converges with the number of round-trips to finite value, for which the procedure stops. It is worth to notice that in the developed model including spatially variable gain saturation it is assumed that the fundamental laser mode is not changed. The main concept consists in application of the analytical solution of a saturable gain (or absorption) equation for a homogeneously broadened medium.

3. Comparison with experimental results

As previously mentioned, the numerical simulation methods are validated by comparison with experimental results. Special care has to be taken when applying the system coupled differential equations defining laser output parameters. In the followings, such comparison of numerical simulation results obtained using the above developed mathematical apparatus performed for two experimental passively Q-switched Nd:YAG lasers are presented: the first based on a rod active medium and the second based on a slab laser active medium.

3.1. Rod laser example

The experimental setup developed in the case of a rod laser active medium numerical simulation results for verifying the simple theory previously presented is designed for measuring the laser output parameters, mainly the FWHM laser pulse time width, at three different lengths of the resonator, keeping unchanged the components of the resonator, including the pumping chamber. As the passive Q-switch cell, a cylindrical LiF:F_2^- crystal is used. The LiF:F_2^- crystal is mounted approximately at one third of the laser resonator. The LiF:F_2^- has no dielectric AR coatings on the optical plane parallel (less than 30″ error) end faces. As observed in Figure 2 the rod laser oscillator setup consists into using a step variable length plane-plane resonator with a high reflectivity mirror (HR in Figure 2) of 99 % reflectivity and an output coupler (OC in Figure 2) manufactured of a quartz plate of about

8 % reflectivity. Into the laser resonator, in order to improve the stability laser output stability, a polarizer made of two 1 mm thick quartz plates placed at Brewster angle versus optical axis is inserted. The pumping system consists of a QUANTRON 104 B reflector made of a cylindrical Quartz block with external and the two internal holes for flash lamp and active medium optical quality polished surfaces. QUANTRON 104 B reflector is made of a colloidal silver layer chemically deposited on the external surface Quartz block surface and protected from oxidation by an electrochemically deposited Ni-Cu layer. An INP 5/60 AI flash lamp mounted on a power source which injected discharge current of about 200 μs duration is used. The adjustable repetition frequency of flash lamp pumping pulses is set at 1 Hz. The active medium is a Ø6×80 mm Nd:YAG laser rod with both ends having AR coatings. The active medium is pumped on 60 mm of its length. The QUANTRON 104 B reflector, flash lamp and laser rod are cooled with flowing de-ionized water.

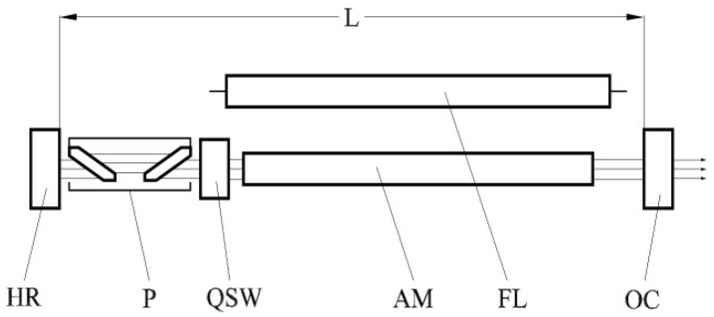

Figure 2. Schematic representation of the rod laser setup. HR - high reflectivity back mirror; P - polarizer; QSW – LiF:F_2^- passive optical Q-switch cell; AM – active medium; FL – flash lamp; OC – output coupler; L – optical resonator length

The laser output is measured with a system composed of:

- laser energy measurement - a thermoelectric GENTEC ED2S energy meter used as the "calibration unit" and a silicon photodiode ROL 021 operated in an inverse polarization mode as a service laser energy monitor;
- laser pulse time shape measurement - an ITT F4014 vacuum photodiode (about 10 ps response time) coupled to a Tektronix 519 oscilloscope (1GHz bandwidth). The response time of this measuring system was estimated to be about 1 ns.

Regarding the LiF:F_2^- crystal used as passive optical Q-switch cell, denoted as Sample C105, it can be mention the fact that it was obtained from a basic crystal with 9 mm diameter and 30 mm length grown in controlled nitrogen atmosphere by Czochralski method. In Table 1, the impurity content concentration of LiF:F_2^- passive optical Q-switch C105 sample, measured by neutron activation method is presented.

Impurity [ppm]										
Type	Na	Cl	K	Ca	Fe	Co	Sc	Zn	La	Pb
II.2	250	1.5	1.7	2.7	185	5.5	2.9	2.5	1.6	2.5

Table 1. The impurity content concentration of investigated LiF:F_2^- passive optical Q-switch C105 sample.

The saturable absorber F_2^- color centers are obtained by "high energy electrons" (about 7 MeV), denoted as "HEE", irradiation at about 1 MRad/h dose and ten Co^{60} γ additional irradiation stages operated at about 1 MRad/h dose. The irradiation procedures applied to Sample C105 are summarized in Table 2 [21].

Sample	Stage 1 [MRad]	Stage 2 [MRad]	Additional [MRad]
C105	250	200	48

Table 2. The irradiation procedures for F_2^- color center formation used for investigated LiF:F_2^- passive optical Q-switch C105 sample.

The end facets of the investigated LiF crystals were optically polished. Optical transmittance measurements were performed on the investigated LiF samples before F_2^- color centers formation by irradiation procedures using a Perkin Elmer Lambda 1050 spectrophotometer. The optical transmittance of clean LiF samples was measured to be of between 0.90 and 0.92. In Table 3, the results of the spectroscopic measurements are summarized.

Sample	Type	T_{Lin}	T_{Lfin}	T_{QswSA}
C105	II.2	0.035	0.899	0.901

Table 3. The spectroscopic characteristics of investigated LiF:F_2^- passive optical Q-switch samples.

The results of numerical simulation for photon density and population inversion density are shown in Figure 3. Experiments proved a good concordance with the simulation. Figure 4 is a plot of measured power density, which fits pretty well with the photon density curve predicted in Figure 3.

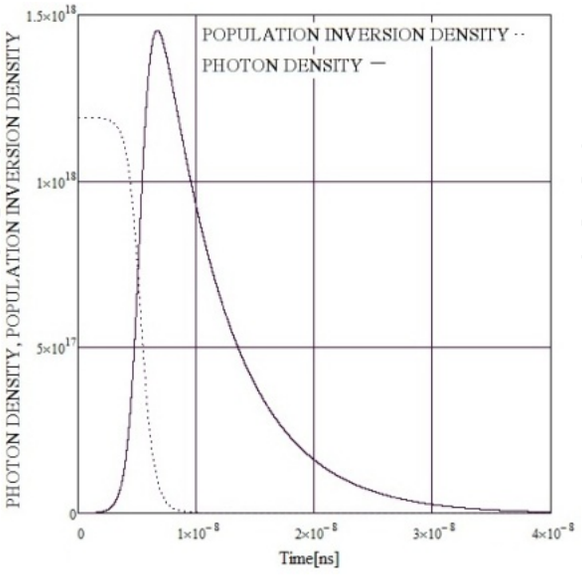

Figure 3. The numerical simulation results for photon density (continuous line) and population inversion density (dotted line).

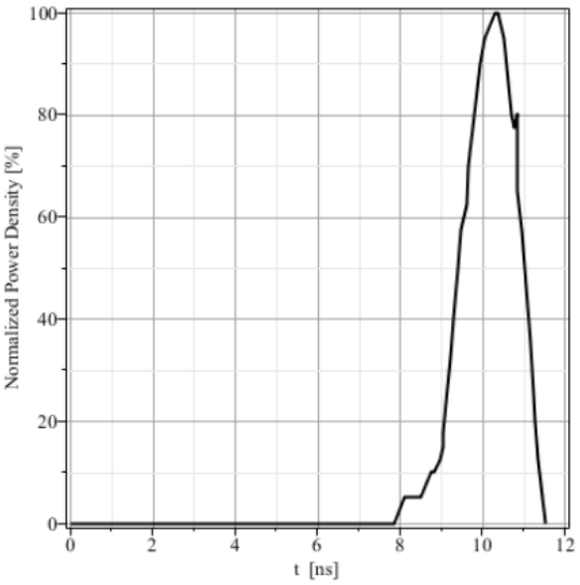

Figure 4. Laser pulse time-shape observed in Q-switching regime for the rod laser oscillator in the case of laser resonator length L = 43.5 cm. Horizontal time division is 2 ns.

3.2. Slab laser oscillator/amplifier example

The use of a slab laser oscillator/amplifier instead of a linear laser resonator offers some remarkable advantages, such as an increased power in smaller volume. Our simulation took into account the schematic presented bellow.

A schematic detail - a cross-section of the pumping chamber - of the investigated Nd:YAG slab oscillator/amplifier laser system setup is shown in Figure 5. The active medium of the investigated laser oscillator/amplifier system is a Nd:YAG crystal slab with sizes of 7 mm × 27 mm ×163 mm with a quite large clear cross-section aperture of 7 mm × 25 mm. The end facets of the active medium are cut and polished at Brewster angle to impose a polarization degree of the laser beam propagating through the laser oscillator/amplifier system. The polarization of the laser light in the case of a passively Q-switched Nd:YAG laser oscillator is useful for the stability of the output parameters, as it is experimentally observed [4]. The slab laser system used a pumping chamber consisting of four krypton flash lamps, 7 mm diameter and 4 inches (101.6 mm) length, mounted into two pairs along the large side surfaces (27 mm ×163 mm) of the Nd:YAG slab active medium. The slab active medium and the flash lamps are cooled using flowing demineralized water. As mentioned in [4], two 2 mm – thick UV cut-off filters (WG360, 360 nm cut-off wavelength) are inserted between the krypton flash lamps and the Nd:YAG crystal slab to prevent UV irradiation of active medium that causes active medium damage by forming color centers and other intrusions. The side un-pumped surfaces of the Nd:YAG crystal slab are thermally insulated by glass plates mounted in direct contact, which serve to dissipate the heat. Accordingly, regarding flash lamp pumping efficiency and considering the spectral match between the Nd:YAG slab active medium absorption bands and the flash lamp light emission, the pumping power transfer coefficient, q_8, is approximated to 2.5%. It is worth to be emphasized that the active

medium of the investigated laser system can be considered as uniformly pumped and, therefore, the pumping rate can be approximated as constant in the cross-sectional area of the active medium, actually in the volume of active medium, within an error of less than 1%.

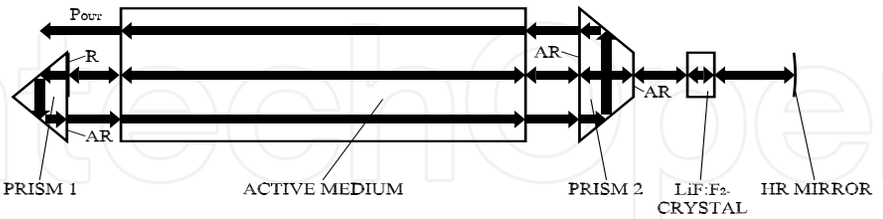

Figure 5. Schematic representation of the slab laser setup. PRISM 1, PRISM 2 – prisms; R – 53 % reflective coating as output coupler; AR – anti-reflective coating; LiF:F_2^- CRYSTAL - passive optical Q-switch cell; ACTIVE MEDIUM – Nd:YAG slab; HR MIRROR – high reflectivity mirror; POUT – outgoing laser beam.

Concerning the approximations considered in defining the system of three coupled differential equations (20) – (22), the experimentally determined time shape of the pump light emitted by the four flash lamps proved the validity of the assumption that the pumping is quasi-continuous. The rise-time and the fall-time of the pump light pulse are short compared to the overall pulse width. This justifies the approximation of using a constant value of R_p during Q-switching process. It is important to mention that the pumping light duration can be varied up to 4 ms, extremely long compared to Nd:YAG fluorescence lifetime (τ_g ~ 250 μs) and to the expected characteristic duration of the investigated Q-switching process (10^{-8} - 10^{-7} s).

The beam aperture in the laser oscillator is one third of the slab width (an area of about 81 mm^2), this value being imposed by the on axis mounted PRISM 2, more exactly, being imposed by the small facet of this prism [4]. The active facets of PRISM 2 are AR-coated to reduce the laser beam parasitic losses. It can be noticed that one third of the Nd:YAG slab active medium is used for the laser oscillator and the rest for the two amplifier stages. The off axis mounted PRISM 1 has a 14 mm hypotenuse, two thirds of the slab active medium width. The upper half of the PRISM 1 hypotenuse has a thin layer of 53% reflectivity. The upper part of the PRISM 1 acts as output mirror (output coupler) for the slab Nd:YAG oscillator. The other optically active facets of the PRISM 1 are AR-coated for the laser wavelength to reduce losses due to laser beam manipulation through the two amplifier stages. The Prism 1 is placed at a distance of about 85 cm from the rear high reflectivity mirror (5 m radius of curvature), denoted as HR MIRROR in Figure 5. Theoretically, the dimensions of the laser resonator output coupler in the transverse plane have to be extremely large compared to the characteristic laser beam transverse dimension, which is mainly imposed by the active medium. Obviously, it is practically impossible to meet this requirement, because a large prism would obstruct the output beam. In our experiment the prism is 7 mm wide, exactly equal to the slab active medium width. This implies

increased scattering losses on the output coupler edges. Therefore the round trip non-saturable dissipative optical loss L will be larger, marking higher losses. In order to effectively use the entire slab active medium volume, the ratio of the width, the hypotenuse of the PRISM 1 and the aperture of PRISM 2 has to be roughly 3:2:1, this being an "on the edge" value [4].

Denoted as samples C326, C327, C328 and C329, four lithium fluoride crystals grown by Czochralski method, were cut and optically polished at dimensions of 10 mm × 10 mm × 40 mm. Each of the developed LiF:F_2^- passive optical Q-switches can be operated in two possible ways: with 10 mm or 40 mm optical length. As indicated in Figure 5, the LiF:F2- passive optical Q-switch uses the 10 mm optical length. They were irradiated by a 1.16 MeV Co60 γ–source at a dose rate of 1 MRad/hour to create the F_2^- color centers, which are the saturable absorber centers of interest to be used in the laser resonator - the final LiF:F_2^- passive optical Q-switch. The impurity content concentration in the raw LiF crystals used for creating LiF:F_2^- passive optical Q-switches are the same as in Table 1. An important feature of the developed LiF:F_2^- passive optical Q-switch is that each of them has four optical active plane facets (two pairs of plane parallel facets).

In Table 4 the parameters determined for the four samples (C326, C327, C328 and C329) of LiF:F_2^- passive Q-switches by spectral measurements are summarized [4]. Here D represents the time integrated Co^{60} γ irradiation dose, T_{in} is the initial (small signal) transmittance, T_{PL} represents the parasitic losses and T_{fin} is the final (saturated) transmittance. The fluorescence lifetime of the saturable absorption centers is τ_a = 75 ns [23]. The ground state absorption cross section of the SA is estimated to be $\tau_a = 1.67 \cdot 10^{-17}$ cm^{-2} [4]. Using these spectral measurements, the F_2^- color centers concentration [F_2^-] can be calculated [4].

Sample	D [MRad]	T_{in}	T_{PL}	T_{fin}	[F_2^-] [cm^{-3}]
C326	150	0.82	0.88	0.87	$4.02 \cdot 10^{15}$
C327	175	0.80	0.91	0.89	$4.19 \cdot 10^{15}$
C328	200	0.75	0.90	0.88	$4.45 \cdot 10^{15}$
C329	225	0.72	0.90	0.88	$4.61 \cdot 10^{15}$

Table 4. The parameters of the tested LiF:F_2^- passive Q-switches.

The transmittance of the lithium fluoride crystals at 1.06 μm (laser wavelength) was measured before and after the F_2^- color centers formation by Co^{60} γ irradiation to accurately determine the LiF:F_2^- passive Q-switches laser functional parameters, as described in [4]. The transmittance spectrogram of a sample of the set of investigated LiF:F_2^- passive optical Q-switches was obtained using a Perkin Elmer Lambda 1050 on a 40 mm optical length LiF:F_2^- sample. The measured transmittance at 1600 nm was considered to be T_{fin} because at this wavelength there is not reported in literature any absorption due to color centers [4]. Here the LiF:F_2^- should to be transparent, as it is recorded in the spectrogram. The measured T_{fin} indicate a low heavy metals impurity concentration. This indicates also a small concentration of colloids formed as by-product of color centers irradiation processing.

The passively Q-switched Nd:YAG slab oscillator/amplifier is basically made up of an oscillator and two amplifier stages, all operating inside the same active medium. It is assumed that the amplification factor of the laser pulses by propagation through the two amplifier stages rise up to about 3.5 - 4.0, increasing with pumping energy up to 1600 J [4]. This is an important issue in performing the numerical simulation of the slab Nd:YAG laser oscillator/amplifier system in the sense that the numeric solution of the coupled rate equations (20) – (22) can provide information about the oscillator stage and the obtained results should be multiplied by the amplification factor (3.5 – 4.0).

The application of the previously presented numerical analysis method consists in performing several successive steps. First of all, the evaluation of the pumping rate, N_{cw}. For both samples considered in this application, the pumping rate of the active medium is evaluated for a 4 ms pumping pulse width and 1040 J pumping pulse energy resulting $R_p = 4.242 \cdot 10^{19}$ cm^{-3}. The population inversion density for the investigated laser system if continuously pumped and operated in free-running regime is defined for the same pumping conditions as $N_{cw} = 1.061 \cdot 10^{16}$ cm^{-3}. The estimated value of N_{cw} is obtained considering σ_g about 230 μs [7]. The Nd:YAG emission cross-section is $\sigma_g = 6.5 \cdot 10^{-19}$ cm^2 [7]. In Table 5, the results of the simulation for laser output parameters, using the mathematical apparatus presented in Section 2, are compared to the experimental data. It can be noticed the fact that the simulated values of E_{out}, σ_{out}, P_{out} and f_{rep} are comparable with the experimental data. σ_p can be considered as fulfilling the necessary condition for multiple laser pulses emission. Considering the value of σ_p (4 ms), the laser emission is therefore quasi continuous. The next step is the simulation of laser pulses repetition frequency, first laser pulse time shape, FWHM pulse width and output energy.

For sample C326 the simulated value of laser pulse repetition frequency is f_{rep} = 75.54 kHz, less than the measured value of 80 kHz, while for sample C329 (see Figure 6) the simulated value of laser pulse repetition frequency is f_{rep} = 25.54 kHz, larger than the measured value of 20 kHz (Figure 7).

Parameter	Unit	Sample C326		Sample C329	
		Simulated	Experimental	Simulated	Experimental
E_{total}	J		26.7		25.0
N_{pulses}	-		334		82
E_{out}	mJ	26	25	105	98.5
σ_{out}	ns	70.77	68.43	28.42	30.90
P_{out}	MW	0.36	0.38	3.75	3.17
f_{rep}	kHz	75.54	80.00	25.14	20.00

Table 5. Summary of laser output parameters experimentally measured and numerically estimated for C326 and C329 samples.

For the sample C326 the simulated FWHM is ~ 72 ns, while the measured value is ~ 68 ns. Figure 8 illustrates the simulated single laser pulse time shape obtained for the sample C329. The simulated FWHM is ~ 31 ns, while the measured value is ~28 ns (see Figure 9).

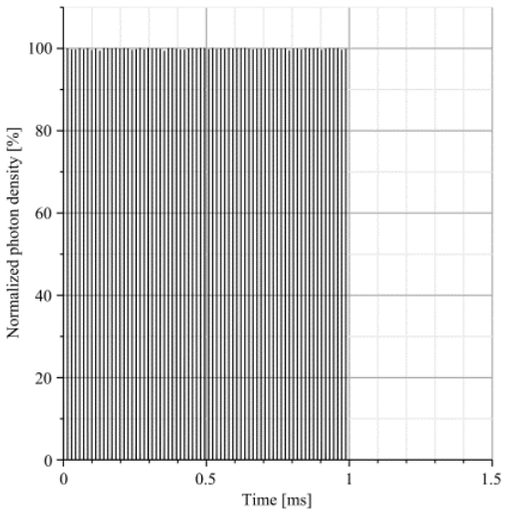

Figure 6. Simulated laser pulses train time-shape.

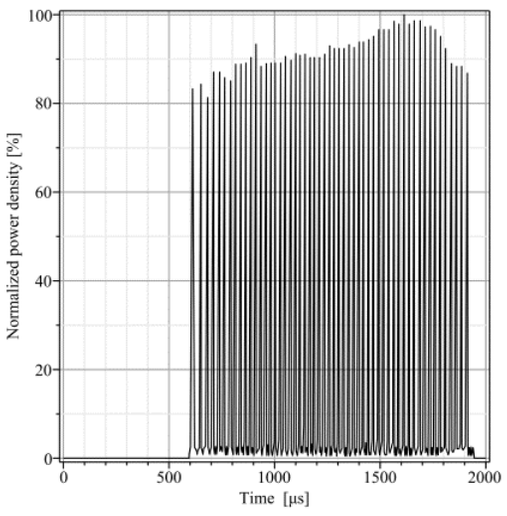

Figure 7. Measured laser pulses train time shape at a pumping pulse width of about 2 ms.

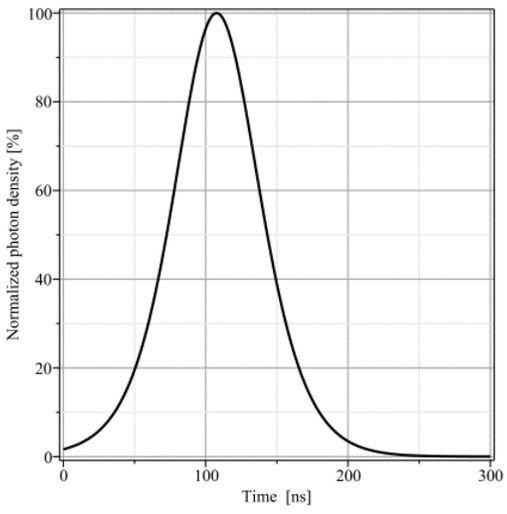

Figure 8. Simulated single laser pulse time shape.

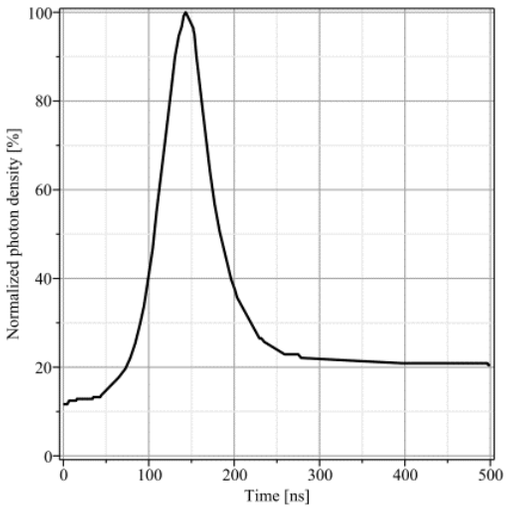

Figure 9. Measured first laser pulse time-shape.

It is worth noticing that several previously defined parameters describing the Nd:YAG slab oscillator/amplifier laser system play an important role in acquiring a certain accuracy of the developed numerical simulation method. As a rule of thumb, the coefficients used for defining the system of coupled rate differential equations (20) – (22) are measured experimentally whenever it is possible. This rule of thumb is valid, directly or through intermediate estimations, for the majority of these coefficients with several exceptions such as R_p, S and L. It is difficult to estimate an accurate value of R_p, in the case of the investigated laser system, because q_g depends on the spectral match between the pumping light emission spectrum of the flash lamps and the absorption lines of the Nd:YAG active medium. This spectral match depends on the neutral glass UV filters used for preventing destruction of the Nd:YAG active medium by the intense UV radiation. In the numerically solving the differential equations (20) – (22) q_g was set to be in the range 0.5% - 1.5%. S is extremely difficult to be accurately estimated because, in principle, it represents a certain percentage of the inverted, pumped Nd:YAG active medium fluorescence emission. S can be evaluated as a coefficient times the initial N_g value, the coefficient being the ratio between the areas subtended by the end apertures, as seen from a middle point of the active medium, on a sphere with the center in this middle point and the radius half of the active medium length. This coefficient has to be "weighted" as considering diffraction effects produced in the laser resonator. In the performed numerical simulations, S is considered as 10^{-6} of N_g initial value. The L coefficient is composed of two parts: the first one due to the non-saturable linear parasitic linear losses of the laser resonator itself and the second one, much smaller, due to the same type of losses of the passive optical Q-switch cell (denoted as T_{PL} in Table 4). For the numerical simulation of the two investigated cases, the samples C326 and C329, the contribution of the laser resonator linear losses was considered as L = 0.1 - 0.3 cm^{-1}.

The simulation results presented in Table 5 are obtained by considering the best fit with experimental data set of q_g, S and L parameters. The q_g, S and L parameters were varied in the previously defined ranges and the developed simulation software was run with these coefficients until the values came close to the measured data. Afterwards, the developed

simulation software was run several times in order to check the obtained results. This procedure suggests a design method for the investigated Nd:YAG laser oscillator/amplifier type, a method relying on the developed simulation procedure. The suggested design method is based on using components, mainly active medium and passive optical Q-switch cells with the parameters previously defined, but with possible different geometrical dimensions, an optimum being found for the best fit of desired output parameters with the set of q_g, S and L parameters.

4. Conclusion

This chapter presents the results obtained in the numerical simulation of a passively Q-switched solid state laser system generating high power, high output energy singular laser pulses or laser pulses trains in pulsed CW or quasi-CW pumping. An important feature of the developed simulation method consists of an analysis of the differences between the first passively Q-switched laser pulse and the next, generated by a CW or a quasi-CW pumped laser system, regarding the recovery condition to the initial state of the passive optical Q-switch cell, which is analyzed in detail for the first time. As far as we know, concerning the passive optical Q-switching, this difference is not reported in literature so far as exhaustively studied. By observing this difference, a method for estimation of laser output pulse parameters is developed. The numerical simulation results are compared to the experimental data and a fairly good agreement between them is observed.

Author details

I. Lăncrănjan
Advanced Study Center–National Institute of Aerospace Research "Elie Carafoli", Bucharest, Romania

R. Savastru, D. Savastru and S. Micloş
National Institute of R&D for Optoelectronics INOE 2000, Magurele, Ilfov, Romania

5. References

[1] Ready JF, Davis J, Berkmanns J, Kugler TR. Lasers for Materials Processing. In: Ready JF. (ed.) LIA Handbook of Laser Materials Processing. Oakland: Magnolia Press; 2001. p27-43.
[2] Steen WM. Laser Material Processing. Berlin, Heidelberg, New York: Springer; 1991.
[3] Misawa H., Juodkazis S. 3D Laser Microfabrication, Weinheim: Wiley-VCH; 2006.
[4] Dong S, Lü Q, Lancranjan I. 220 W Average Output Power From a Q-Switching Nd: YAG Slab Laser with a LiF: F_2^- Crystal. Optics and Laser Technology 1993; 25(3) 175-178.
[5] Siegman AE. Lasers, Sausalito: University Science Books; 1986.
[6] Mercer CJ, Tsang YH, Binks DJ. A Model of a QCW Diode Pumped Passively Q-Switched Solid State Laser. Journal of Modern Optics 2007; 54 (12) 1685-1694.

[7] Koechner W. Solid State Laser Engineering, Berlin: Springer; 2006.
[8] Fan TY, Byer RL. Diode Laser-Pumped Solid State Lasers. IEEE Journal of Quantum Electronics 1988; 24 (6) 895-912.
[9] Laporta P, Brussard M. Design Criteria for Mode Size Optimization in Diode-Pumped Solid-State Lasers. IEEE Journal of Quantum Electronics 1991; 27(10) 2319-2326.
[10] Siegman AE. New Developments in Laser Resonators. In: Holmes DA (ed.) Optical Resonators, 1990, Proceedings of SPIE vol. 1224; 2-14.
[11] Degnan JJ. Optimization of Passively Q-Switched Lasers. IEEE Journal of Quantum Electronics 1995; 31(11) 1890-1901.
[12] Degnan JJ. Theory of the Optimally Coupled Q- Switched Laser. IEEE Journal of Quantum Electronics 1989; 25(2) 214-220.
[13] Kuo YK, Birnbaum M, Chen W. Ho:YLiF4 Saturable Absorber Q-Switch for the 2-◎m Tm, Cr:Y3Al5O12 Laser. Applied Physics Letters 1994; 65(24) 3060-3062.
[14] Kuo YK, Huang MF, Birnbaum M. Tunable Cr^{4+}:YSO Q-Switched Cr:LiCAF Laser. IEEE Journal of Quantum Electronics 1995; 31(4) 657-663.
[15] Kuo YK, Birnbaum M. Passive Q-Switching of the Alexandrite Laser with a Cr^{4+}:Y_2SiO_5 Solid-State Saturable Absorber. Applied Physics Letters 1995; 67(2) 173-175.
[16] Kuo YK, Birnbaum M. Ho:YVO4 Solid-State Saturable Absorber Q Switch for 2-◎m Tm,Cr:$Y_3Al_5O_{12}$ Laser. Applied Optics 1996; 35(6) 881-884.
[17] Kuo YK, Chen W, Stultz RD, Birnbaum M. Dy^{2+}:CaF_2 Saturable-Absorber Q Switch for the Ruby Laser. Applied Optics 1994; 33(27) 6348-6351.
[18] Kuo YK, Birnbaum M, Unlu F, Huang MF. Ho:CaF_2 Solid-State Saturable Absorber Q-Switch for the 2-◎m Tm,Cr:$Y_3Al_5O_{12}$ Laser. Applied Optics 1996, 35(15) 2576-2579.
[19] Kuo YK, Lee S, Unlu F, Huang MF, Birnbaum M, Fuqua PD, Dunn B. Solid State Polymer Dye Q-Switch for Cr:LiCAF, Alexandrite, and Ruby Lasers. Electronics Letters 1996; 32(23) 2146-2148.
[20] Kuo YK, Chen HM. Cr:YSO Saturable Absorber for the Three-Level Cr:$BeAl_2O_4$ Laser at 680.4 nm, Japanese Journal of Applied Physics 2000; 39(12A) 6574-6575.
[21] Y. K. Kuo, H. M. Chen, J. Y. Chang, Numerical study of the Cr:YSO Q switched ruby laser, Opt. Eng., 9 (2001) 2031-2035.
[22] Kuo YK, Chen HM, Chang Y. Numerical Study of Passive Q switching of a Tunable Alexandrite Laser with a Cr:Y2SiO5 Solid-State Saturable Absorber. Applied Optics 2001; 40(9) 1362-1368.
[23] Zayhowski JJ, Kelley PL. Optimization of Q-Switched Lasers, IEEE Journal of Quantum Electronics 1991, 27(9) 2220-2225.
[24] Lancranjan I, Miclos S, Savastru D, Popescu A. Numerical Simulation of a DFB-Fiber Laser Sensor (II) - Theoretical Analysis of an Acoustic Sensor. Journal of Optoelectronics and Advanced Materials 2010; 12 (12) 2456-2461.
[25] Lancranjan I, Miclos S, Savastru D, Popescu A. Numerical Simulation of a DFB-Fiber Laser Sensor (I). Journal of Optoelectronics and Advanced Materials 2010; 12 (8) 1636-1645.

[26] Lancranjan I, Miclos S, Savastru D. Numerical Simulation of a Passive Optical Q – Switched Solid State Laser - High Brightness Nd:YAG Laser Case. Journal of Optoelectronics and Advanced Materials 2011; 13 (5-6) 477-484.
[27] Basiev TT, Mirov SB, Osiko VV. Room-Temperature Color Center Lasers. IEEE Journal of Quantum Electronics 1988; 24 (6) 1052-1069.
[28] Kapoor R, Mukhopadhyay PK, George J. A New Approach to Compute Overlap Efficiency in Axially Pumped Solid State Lasers. Optical Express 1999; 5(6) 125-133.
[29] Zayhowski JJ. Thermal Guiding in Microchips. In: Dube G, Jensen HP.(eds.) OSA Proceedings on Advanced Solid State Lasers 1990; 9-13.
[30] Innocenzi ME, Yura HT, Fincher CL, Fields RA. Thermal Modeling of Continuous-Wave-Endpumped Solid-State Lasers. Applied Physics Letters 1990; 56(19) 1831-1833.
[31] Zhang X, Zhao S, Wang Q, Ozygus B, Weber H. Modeling of Passively Q-Switched Lasers. Journal of Optical Society of America B 2000; 17 (7) 1166-1175.
[32] Salin F, Squier J. Gain Guiding in Solid State Lasers. Optics Letters 1992; 17(19) 1352-1354.
[33] Magni V, Cerullo G, De Silvestri S. Closed Form Gaussian Beam Analysis of Resonators Containing a Kerr Medium for Femtosecond Lasers. Optics Communications 1993; 101(5-6) 365-370.
[34] Kemp AJ, Conroy RS, Friel GJ, Sinclair B. Guiding Effects in Nd:YVO_4 Microchip Lasers Operating Well Above Threshold. IEEE Journal of Quantum Electronics 1999; 35(4) 675-681.
[35] Serrat C, van Exter MP, van Druten NJ, Woerdman JP. Transverse Mode Formation in Microlasers by Combined Gain- and Index-Guiding. IEEE Journal of Quantum Electronics 1999; 35(9) 1314-1321.
[36] Denchev O, Kurtev S, Petrov P. Modes of Unstable Resonators with a Saturable Gain Guide. Applied Optics 2001; 40(6) 921-929.
[37] Grace EJ, New GH, French PMW. Simple ABCD Matrix Treatment for Transversely Varying Saturable Gain. Optics Letters 2001; 26(22) 1776-1778.
[38] Barry DA, Parlange JY, Li L, Prommer H, Cunningham CJ, Stagnitti F. Analytical Approximations for Real Values of the Lambert W-Function. Mathematics and Computers in Simulation 2000; 53(1-2) 95-103.